Scanning tunneling microscopy contrast in lateral Ge-Si nanostructures on Si(111)-$\sqrt{3}\times\sqrt{3}$-Bi

Josef Mysliveček,[1,2,*] Filip Dvořák,[1] Anna Stróżecka,[2,†] and Bert Voigtländer[2]
[1]*Faculty of Mathematics and Physics, Charles University, V Holešovičkách 2, Praha 8, Czech Republic*
[2]*Institut für Bio- und Nanosysteme, Forschungszentrum Jülich, 52425 Jülich, Germany*
(Received 1 February 2010; revised manuscript received 4 June 2010; published 22 June 2010)

We investigate the origin of scanning tunneling microscope (STM) contrast in lateral Ge-Si nanostructures prepared on the Si(111)-$\sqrt{3}\times\sqrt{3}$-Bi surface [M. Kawamura, N. Paul, V. Cherepanov, and B. Voigtländer, Phys. Rev. Lett. **91**, 096102 (2003)]. At low sample bias, the voltage-dependent apparent height difference between Si- and Ge-terminated areas in STM images corresponds exceptionally well to the difference in voltage-integrated scanning tunneling spectroscopy (STS) curves measured in Si- and Ge-terminated areas. The STS curves and the STM contrast reflect both differences in local density of states and in tip-induced effects in Si- and Ge-terminated areas. At higher bias voltage, the tunneling into unoccupied states on Ge-terminated areas is strongly influenced by lowering of the local height of the tunneling barrier with respect to Si. The lowering of the local tunneling barrier height vanishes for the occupied states and can be traced back to different tip-induced band bending on Si- and Ge-terminated areas.

DOI: 10.1103/PhysRevB.81.245427 PACS number(s): 73.20.At, 68.47.Fg, 68.37.Uv, 68.37.Ef

I. INTRODUCTION

Chemical contrast in scanning tunneling microscopy (STM) is a complex issue. The expression for the tunneling current I_t is very straightforward: I_t is proportional to the local density of states (LDOS) of the surface, at the position of the STM tip,[1] integrated between surface and tip Fermi levels.[2] Unfortunately, the most important contributions to I_t, the LDOS, and the local height of the tunneling barrier influencing the projection of the LDOS on the tip, often do lack the chemical specificity. Electron states relevant for the STM lie within 5 eV from the surface Fermi level $E_{F,S}$ in valence and/or conduction bands, where the large energy shifts due to delocalization and the rehybridization prevents identifying energy levels of single constituent atoms. The local tunneling barrier is modified by a charge redistribution between the surface and the bulk and can be affected by a presence of different surface atoms, however, with little relation to their chemical nature. Obtaining chemical information in STM measurements is thus more an exception than the rule.

In spite of this, there exists a notable class of semiconductor,[3] metal,[4] and mixed[5] binary systems in which two types of atoms constituting the surface can be distinguished and localized on atomic level based on STM contrast. In such systems, STM measurements yield important information on the stoichiometry and space correlations in surface alloys[6–8] or on the morphology of different phases in systems with limited intermixing.[9,10] The origin of the STM contrast is specific to each such system and can be followed both experimentally and theoretically.[6–10] Most explanations, however, fit in agreement with the definition of I_t to one of two prototypical cases: the presence of different chemical species on the surface strongly influences the LDOS (Ref. 11) and/or the local work function.[12]

One of the most studied binary systems with a vast application potential is Ge-Si.[13] The structural and the chemical similarities of Ge and Si make obtaining STM contrast in Ge-Si systems difficult, especially at submonolayer Ge coverage, where Ge atoms substituting Si surface atoms barely change the local geometry and electronic properties.[14] The STM contrast can be enhanced in the presence of a third species on Ge-Si surface: Cl (Ref. 15) or Bi (Ref. 16). Cl acts as a simple "stain" for distinguishing Ge and Si dangling bonds on Ge/Si(001)-2×1 surface, while Bi is a surfactant in Ge-Si(111) heteroepitaxy.[17,18] Bi forms a floating monolayer (ML) on a growing Ge-Si surface, and, in addition to providing the STM contrast between the underlying Ge and Si atoms, it greatly influences the growth kinetics of Ge on Si(111) (Refs. 18 and 19) and suppresses the Ge-Si intermixing.[16,20] The favorable properties of Bi allowed preparation and characterization by STM of Ge-Si nanowires and nanorings with dimensions on the one-digit nanometer scale,[16,21] identification and quantitative analysis of Ge-Si intermixing mechanisms on single-atom level,[20,22] and determination of anisotropic step propagation rates in Ge-Si epitaxy,[23] all on the Bi-terminated Si(111) surface.

Here we present a combined STM and scanning tunneling spectroscopy (STS) study of the STM contrast between submonolayer Ge and Si on the Si(111) surface terminated by 1 ML Bi [Si(111)-$\sqrt{3}\times\sqrt{3}$-Bi, 1 ML Bi=2.36×10^{15} cm^{-2})].[24] We measure the STM height difference between clean and Ge-terminated areas on this surface as a function of the tunneling voltage V_s (sample bias). For $|V_s|<3$ V we find an unexpectedly good correlation between the voltage-dependent height difference and the difference in voltage-integrated STS curves confirming the predominantly electronic character of the observed contrast.[25] Especially, a strong onset of STM contrast for tunneling in unoccupied sates ($V_s\approx2$ V) is correlated with a pronounced peak in the Ge STS that can be assigned to LDOS. Further, the tunneling in unoccupied states over Ge areas features a lower local height of the tunneling barrier than over Si areas. The difference in the local tunneling barrier height is the main contribution to the maximum height difference observed at $V_s>4$ V where localized electron states form between the sample and the STM tip.[26,27] In occupied states, the difference in local tunneling barrier height vanishes. We show that

the observed difference of the local height of the tunneling barrier is caused by the penetration of the electric field of the STM tip into the bulk of the sample.[28,29] This so-called tip-induced band bending is smaller on Ge-terminated areas and indicates that these areas screen the electric field of the tip more effectively.

II. EXPERIMENTAL

We performed the measurements in ultrahigh vacuum on a commercial low-temperature STM. The STM tips were electrochemically etched from a polycrystalline W wire and treated *in situ* on a Pt(111) surface to ensure the metallic character of the tip.[30] We used degenerately *n*-doped Si(111) substrates $(1.6\times10^{19}$ cm^{-3} As).[31] Substrates were flashed by dc current to 1220 °C to obtain a clean Si(111)-7×7 surface. The surface was terminated by Bi in Bi flux >1 ML/min and substrate temperature ramping from 600 °C down to 400 °C for 30 min. This ensures a complete 1 ML Bi coverage and a perfect Si(111)-$\sqrt{3}\times\sqrt{3}$-Bi.[21] 0.3 bilayer (BL) Ge were deposited at 400 °C and 0.2 BL/min under continuing Bi flux (1 BL Ge$=1.57\times10^{15}$ cm^{-2}). This ensures decoration of pre-existing Si step edges by Ge nanowires and minimal intermixing with Si.[20]

The voltage-dependent height difference between Ge and Si areas was measured in two ways. At $|V_s|<4$ V (Sec. III A), STM images of neighboring Si and Ge areas were taken at $I_t=0.1$ nA and varying V_s. The Ge-Si height difference was obtained by fitting parallel planes to Ge and Si areas. At a particular V_s, several STM images have been taken that allowed eliminating the thermal drift and obtaining the voltage-dependent tip-sample separation s in addition to the Ge-Si height difference for most V_s. The zero of the tip-sample separation was estimated in a separate experiment based on an average distance an unbiased tip needed to travel toward the sample before inducing a surface change. At $V_s\in(2,10)$ V (Sec. III C), the tip heights over Ge and Si were obtained from point measurements of s as a function of V_s at $I_t=0.1$ nA. The tip height records were offset at their starting point ($V_s=2$ V, $I_t=0.1$ nA) by a Ge-Si height difference obtained by fitting of parallel planes in a corresponding STM image, and the Ge-Si height difference for $V_s\in(2,10)$ V was determined.

The LDOS for Ge and Si areas at $|V_s|<3$ V (Sec. III B) was inferred from measurements of scanning tunneling spectra after Ref. 32. In measuring STS on semiconductors with a surface band gap [as is the case of Si(111)-$\sqrt{3}\times\sqrt{3}$-Bi, see Refs. 24 and 25] a problem arises with proper capturing of all features in the STS spectra, because the I_t and the primary STS signal dI_t/dV_s are dropping by several orders of magnitude in the proximity of the band edges. Reference 32 suggests compensating this sensitivity loss by decreasing the tip-sample distance with decreasing $|V_s|$, $ds=-\alpha d|V_s|$. For presentation, the dI_t/dV_s measured with varying s is "normalized" by dividing with $\overline{I_t/V_s}$. The overline indicates "broadening" of the I_t/V_s by Fourier low-pass filtering in the voltage domain. The normalization by $\overline{I_t/V_s}$ have proved very effective in compensating the exponential dependence of dI_t/dV_s on both the s and V_s.[33,34] Thus, the STS expressed as $(dI_t/dV_s)/\overline{(I_t/V_s)}$ is, effectively, a tip-sample distance invariant.[32] To measure the STS with varying s, we stabilize the STM feedback to $I_t^0=0.1$ nA, $V_S^0=3$ V, switch it off and measure the I_t and dI_t/dV_s as a function of V_s. For measuring dI_t/dV_s we are using a lock-in technique and a modulation of V_s with a frequency of several hundred hertz and amplitude on the order of 10 mVpp.

At $V_s\in(2,10)$ V (Sec. III C), outside of the band-gap region, a second technique of measuring STS spectra has been used. The spectra over Ge and Si areas were expressed as a plain derivative dI_t/dV_s. The measurement proceeded with feedback on, stabilized at $I_t=0.1$ nA, and V_s ramping from 2 to 10 V.[26,27] The lock-in frequency was set higher than the feedback bandwidth. Simultaneously, the above-mentioned measurement of the voltage-dependent tip height over Ge and Si areas was performed.

In Sec. III C we are discussing the V_s dependence of the local tunneling barrier height. We are doing this in terms of the inverse decay length κ of the tunneling current I_t, $I_t=\exp(-2\kappa s)$.[35] The V_s dependence of κ for Ge and Si areas was determined from the exponential increase in I_t after stabilizing the feedback to $I_t^0=0.1$ nA, switching it off and reducing the tip height by 1 Å.

The measurements were performed at low temperature $T=7$ K. The advantages of the low-temperature measurements are a negligible drift and a good stability of the STM tip. Actually, the presented measurements of the height difference, STS, and decay length (cf. Figs. 2, 3, and 6) were for the best possible correlation all made with a single tip and without a detectable tip and/or surface change. STS and height difference data for $V_s\in(2,10)$ V (cf. Fig. 5) were selected from several measurements with different tips to ensure the best correspondence of the tip work function within all experimental data presented in this work.

All presented experimental data are averages over 10–20 measurements at defect-free positions within Ge or Si areas, respectively. Sizes of symbols in the presented graphs are larger than the corresponding statistical error.

III. RESULTS AND DISCUSSION

A. STM topography and height difference

First, we re-examine imaging of the Si(111)-$\sqrt{3}\times\sqrt{3}$-Bi surface with STM in atomic resolution. There has been a certain controversy in literature regarding the actual content of Bi (1/3, 2/3, or 1 ML) on this surface[36–38] caused by observations of three different patterns in STM, the trimer, the honeycomb, and the monomer.[36] This controversy seems to have been resolved by a recent theoretical work[24,25] predicting that all three patterns be observable on the Si(111)-$\sqrt{3}\times\sqrt{3}$-Bi surface with 1 ML Bi: a pronounced trimer in occupied states,[24] honeycomb in lower energy unoccupied states,[24,25] and a smeared trimer (apparent monomer) in higher energy unoccupied states.[25]

We show the V_s dependence of the STM pattern of the Si(111)-$\sqrt{3}\times\sqrt{3}$-Bi surface in Fig. 1(a)—trimer, Fig. 1(b)—honeycomb, and Fig. 1(c)—apparent monomer. We observe the ordering of the patterns in energy as predicted theoretically. The trimer is observed at $V_s\in(-4,-1.9)$ V, the hon-

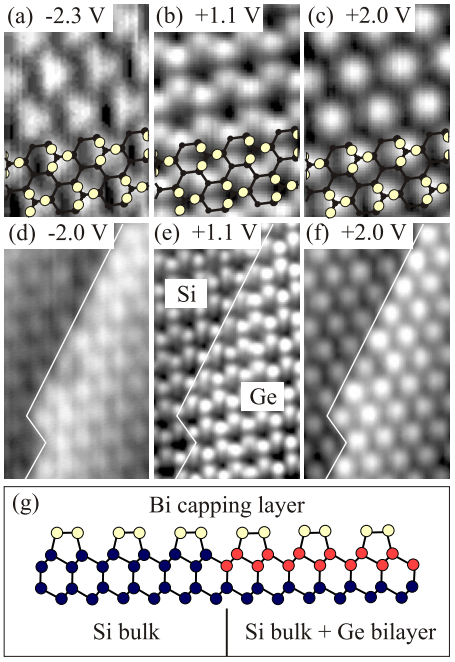

FIG. 1. (Color online) (a)–(c) STM topographs of clean Si(111)-$\sqrt{3}\times\sqrt{3}$-Bi as a function of sample voltage. Tunneling current 0.5 nA, image width 20 Å. (d)–(f) The same for a lateral boundary between clean (Si) and Ge-terminated (Ge) Si(111)-$\sqrt{3}\times\sqrt{3}$-Bi. Image width 40 Å. (g) Schematic side view of the Si-Ge lateral boundary.

eycomb at $V_s \in (-1.9,-1.3)$ V and $V_s \in (0.9,1.9)$ V, and the monomer at $V_s \in (1.9,2.7)$ V. The voltage ranges are indicated schematically in Fig. 3. At $V_s \in (-1.3,0.9)$ V no stable imaging is possible. At $V_s > 3$ V the surface appears smooth without any pattern. We thus conclude that the surface in our experiment is the Si(111)-$\sqrt{3}\times\sqrt{3}$-Bi surface with 1 ML Bi. The structure of this surface is a milkstool model with Bi trimers on top of T_4 sites of the underlying Si(111).[24] We overlay a schematic of this structure with Bi atoms (light) on a Si bilayer (black) in Figs. 1(a)–1(c). According to Ref. 24, surfaces with 1/3 ML Bi can also be stable, however, our previous experiments indicate that the surfaces with less than 1 ML Bi tend to develop a mosaic of Bi and Si atoms rather than a homogeneous pattern.[21]

Figures 1(d)–1(f) show the STM patterns across a boundary between clean (Si) and Ge-terminated surfaces. The boundary is located at a position of an original step edge on Si(111)-$\sqrt{3}\times\sqrt{3}$-Bi surface decorated by a bilayer of Ge (below Bi). On Ge, the ordering of the patterns in energy is the same as on Si. The transitions between patterns with changing V_s occur within ± 0.1 V from the transitions on Si. This observation confirms the previous assumption[16] and the theoretical prediction[25] that the Ge areas have the same milkstool structure as the Si areas but with the last Si bilayer substituted by Ge. A corresponding side view of the lateral Ge-Si boundary is shown in Fig. 1(g). The *only* difference between Ge and Si in the STM images across V_s is thus the apparent height. The height difference is effective on the length scale corresponding to the distance between neighboring Bi trimers.

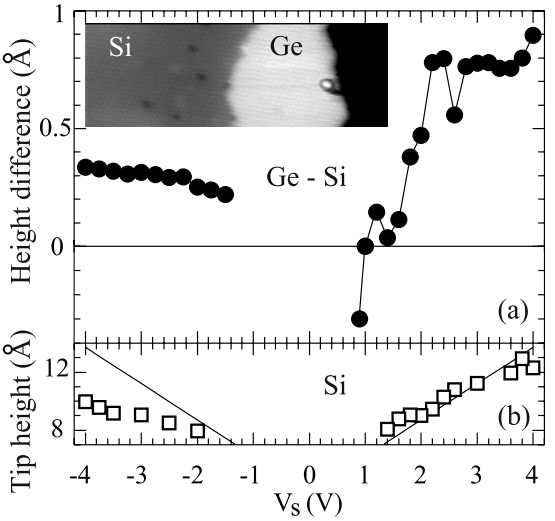

FIG. 2. (a) Apparent height difference between clean (Si) and Ge-terminated (Ge) Si(111)-$\sqrt{3}\times\sqrt{3}$-Bi measured in STM as a function of sample voltage. Tunneling current 0.1 nA. The line represents a guide to the eyes. (b) Corresponding tip height over Si. Tunneling current 0.1 nA. The line represents a tip trajectory for STS measurements [cf. Fig. 3(a)]. Inset: STM topograph of the measurement area. Sample voltage 2.2 V, image width 40 nm.

We show the height difference measured between Ge and Si areas as a function of V_s in Fig. 2(a). For most voltages, Ge appears higher than Si. The height difference increases with increasing $|V_s|$. In occupied states, the increase is monotonic and the height difference of 0.3 Å is achieved. In unoccupied states, Ge appears lower than Si for the smallest voltage V_s=0.9 V. The Ge-Si height difference increases rapidly to 0.8 Å at V_s=2.2 V and further to almost 1 Å at V_s=4 V. The increase shows pronounced kinks at $V_s = (1.4,1.9,2.6)$ V. The observed height difference is significantly larger than the outward relaxation of the positions of Bi atoms on Ge with respect to Bi atoms on Si of 0.1 Å determined in an *ab initio* calculation of Ref. 25. This shows that the height difference is predominantly of electronic origin.[25]

Parallel to the height difference between Ge and Si areas, a tip-sample distance on the Si areas has been determined. We show the tip-sample distance on Si in Fig. 2(b). We observe a monotonic increase in s with increasing $|V_s|$ in both occupied and unoccupied states. A small modulation of s with V_s shows no apparent correlation with the Ge-Si height difference in Fig. 2(a).

B. Height difference vs LDOS

The most cited reason for the height difference in STM in binary systems is a difference in the LDOS.[6–9,11] We discuss the difference between the Ge LDOS and Si LDOS based on the measurement of STS in the corresponding surface areas. The STS at $|V_s| < 3$ V was measured with disabled feedback and varying tip-sample distance. The tip trajectory during STS measurement is plotted in Fig. 2(b). The slope of the trajectory α=2.5 Å/V allows clear resolving of the STS features for all V_s, and, especially in the unoccupied states, it

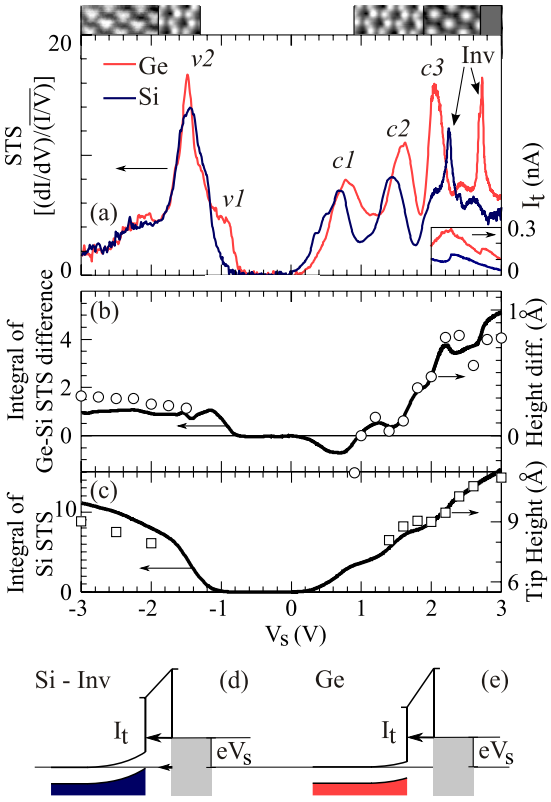

FIG. 3. (Color online) (a) STS measured over clean (Si) and Ge-terminated (Ge) Si(111)-$\sqrt{3}\times\sqrt{3}$-Bi. Valence band ($v1$,$v2$) and conduction band ($c1$-$c3$) LDOS features and a bulk inversion (Inv) are labeled. Inset: tunneling current change corresponding to the bulk inversion. (b) Line: integral of the difference between Ge STS and Si STS with respect to voltage. Points: the voltage dependence of the STM contrast from Fig. 2(a). (c) Line: integral of the Si STS with respect to voltage. Points: the voltage dependence of the Si tip height from Fig. 2(b). [(d) and (e)] Different positions of Inv in Si and Ge STS indicate a weaker tip-induced band bending in Ge. Under such conditions with increasing V_s, the inversion will be observed first in Si: compare (d) and (e) for the same V_s in Ge and Si.

corresponds well to the tip height for STM imaging at I_t = 100 nA. We present the STS in a normalized form, STS $=(dI_t/dV_s)/\overline{(I_t/V_s)}$ which is a tip-sample distance invariant (see Sec. II).

STS curves measured over Ge and Si areas are shown in Fig. 3(a). As expected based on the similarity of Ge and Si structures (Fig. 1), the differences between the spectra are moderate. A shape of the spectra closely resembles the LDOS calculated for Si(111)-$\sqrt{3}\times\sqrt{3}$-As surface in Ref. 39. We thus assume that the STS spectra are dominated by LDOS contributions and label the most pronounced LDOS features in unoccupied states $c1$-$c3$ and in occupied states $v1$, $v2$. A theoretical prediction of LDOS in Si(111)-$\sqrt{3}\times\sqrt{3}$-Bi is not available at present, however, in Ref. 25 a prediction of band offsets between Ge and Si areas has been made. In agreement with this prediction, our measurements show an offset of Ge conduction- and valence-band edges (CBM and VBM) to higher energies with respect to Si, smaller at the CBM and larger at the VBM.

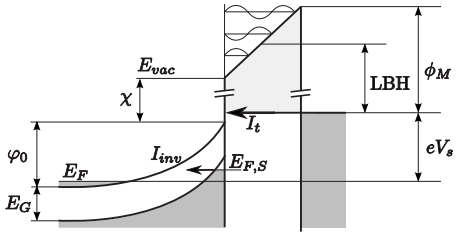

FIG. 4. Schematic of the tunneling into unoccupied states on a degenerately n-doped semiconductor. In the semiconductor (left, dark gray), the symbols are: bulk Fermi level E_F, band gap E_G, vacuum level E_{vac}, electron affinity χ, tip-induced band banding φ_0, and surface Fermi level $E_{F,S}>E_F$ for nonequilibrium tunneling. In the metal (right, dark gray), the symbols are: sample bias eV_s and tip work function ϕ_M. The tunneling current I_t is passing a local tunneling barrier with a height LBH (light gray). The inversion current I_{Inv} is passing the space charge layer between valence and conduction bands. Above E_{vac}, localized electron states in the tunneling gap are indicated that cause resonances in STS for $eV_s>E_{vac}$.

The labeled LDOS features in Si and Ge STS have a comparable peak width of 0.3–0.4 eV. In both Ge and Si STS, there appears a peak that is significantly narrower. Closer inspection of the data reveals that this peak originates from differentiating a step change in I_t observed at V_s = 2.3 V for Si and 2.7 V for Ge areas [inset of Fig. 3(a)]. A steplike change with a comparable magnitude, albeit at opposite polarity of V_s, has been observed in Ref. 29 and interpreted as an onset of the bulk inversion caused by the tip-induced band bending. The polarity of such effect is expected to change between p-doped (as in Ref. 29) and n-doped substrates (the present work).

In analogy with Ref. 29, we assign the narrow peaks in Si and Ge STS to the onset of the bulk inversion caused by the tip-induced band bending. We label the peaks "Inv" in Fig. 3(a). On n-doped semiconductor substrates, tunneling into unoccupied states induces band bending that increases the energy of the electrons in the subsurface region (cf. Fig. 4). The band bending increases with increasing V_s until the energy of the electrons in the VBM at the surface becomes higher than the energy of the electrons on the bulk Fermi level. Under such conditions, a new current channel will open between the sample surface and the bulk, and a steplike change in I_t may be observed [Fig. 3(d)]. The fact that this steplike change appears at higher V_s on the Ge areas than on the Si areas indicates that for the same V_s, the tip-induced band bending is smaller on the Ge areas than on the Si areas [Figs. 3(d) and 3(e)], and that the Ge areas screen the electric field of the tip more effectively.

The observation of the bulk inversion indicates that the STS curves include non-density-of-states features. Apart from the inversion and the differences in tip-induced band bending between Ge and Si areas also effects related to electron-transport problems in STS at low temperatures may be observed. The effects include broadening of the surface band gap in STS and shifting of peaks in STS to higher energies.[31] For identifying these effects, we refer to an *ab initio* calculations of the Si(111)-$\sqrt{3}\times\sqrt{3}$-Bi surface that pre-

dict a free-electronlike surface state protruding from CBM 0.2 eV into the bulk band gap, and reducing the surface band gap with respect to bulk band gap.[24] The bulk band gap of Si at $T=7$ K is about 1.15 eV, and the expected surface band gap of 0.95 eV for Si(111)-$\sqrt{3}\times\sqrt{3}$-Bi corresponds well to the band gap observed in our STS measurements. However, standing electron waves in STM images[40] indicating the free-electronlike surface state appear at energies well outside the band gap [$V_s \in (0.9, 1.4)$ V].[41] This indicates a significant shift of the spectral features in the present STS measurement with respect to their real energies.[31]

In spite of the various effects causing deviations of the measured STS from the real LDOS, a closer inspection of the measured Ge and Si STS [Fig. 3(a)] yields differences that correlate with the V_s dependence of the STM contrast. In the following, we will be using an assumption that the peak heights observed in our STS measurements are not arbitrary but related to the magnitude of the LDOS. This assumption is not valid in general,[42] but may be of relevance for comparative measurements on very similar surfaces as in the present study.

For most V_s, the measured Ge STS is higher than the Si STS. The difference of STS is higher for unoccupied states, in agreement with the V_s dependence of the STM contrast. At certain values of V_s, the Si STS becomes locally higher than the Ge STS or approaches it closely. At such V_s, kinks are observed in the STM contrast [$V_s=(1.4, 1.9, 2.6)$ V]. This indicates a close correlation between the measured STS and the height difference. This correlation becomes clearly apparent when calculating an integral of the difference between the Ge and Si STS with respect to voltage, $\int_0^{V_s} \mathrm{STS}_{\mathrm{Ge}}(V) - \mathrm{STS}_{\mathrm{Si}}(V) dV$. The integrated curve is plotted in Fig. 3(b), superimposed with the points of experimental dependence of STM contrast from Fig. 2(a). The curve reproduces all features observed in the V_s dependence of the STM contrast between $V_s=\pm 3$ V including the inversion of Ge-Si contrast at $V_s=0.9$ V or the kinks at $V_s>0$ V and shows even a considerable quantitative agreement with the height-difference data.

This is a somewhat surprising result given that integrating the difference in STS is an *ad hoc* construction, albeit inspired by the fact that LDOS contributions to I_t integrate between 0 V and V_s (Ref. 35), and that the employed normalization removes the dependence of STS on the tunneling barrier height (Sec. II). It is interesting to note that the integral of STS correlates very well also with the tip-sample distance. We show this effect in Fig. 3(c), where the integral of Si STS is plotted and superimposed with the points of experimental dependence of the tip-sample distance on Si from Fig. 2(b). Linearly transformed, the integral of Si STS reproduces to a great extent both the V_s dependence of the tunneling height, and its modulation at positive V_s that can be ascribed to contributions from $c2$ and $c3$ peaks in Si STS.

In fact, there seems to be a unique correspondence between the STS after Refs. 32–34 (tip-sample distance invariant) and the tip-sample distance. The physical background and the general applicability of this correspondence may require a further study. However, in our particular case the observed correspondence allows us to conclude, that the height difference between Ge and Si areas on the Si(111)-$\sqrt{3}\times\sqrt{3}$-Bi surface, and for $|V_s|<3$ V, is predominantly determined by the STS *as seen by the* STM, including both true LDOS contributions, and other effects, particularly due to the tip-induced band bending and electron-transport problems at low temperatures.

We propose that the true LDOS differences between Ge and Si areas are determining the overall shape of the voltage-dependent height difference, especially the onset of Ge-Si height difference in unoccupied states. True LDOS differences can be identified as Ge STS peaks that have a small or no counterpart in the Si STS spectra. This is the case of the peaks c_3 and v_1 in Fig. 3(a).[43] The position of the c_3 peak correlates well with the strong onset of the Ge-Si contrast at $V_s=2$ V. Similarly, the v_1 peak is the most pronounced contribution to the height difference in occupied states. The appearance of the v_1 peak corresponds well to a theoretical prediction of a pronounced VBM state on Ge areas.[25] The v_1 VBM state,[25] and, supposedly, the c_3 state as well, are localized in the vicinity of the Ge atoms, and allow distinguishing Ge and Si atoms on the Si(111)-$\sqrt{3}\times\sqrt{3}$-Bi surface on the lateral scale of single trimers [Figs. 1(d)–1(f)] and measuring the Ge content in the Ge-Si surface alloys based on the STM contrast.[20]

The fine structure (kinks) of the voltage-dependent height difference is determined by mutual positions of Ge and Si c_1, c_2, and Inv peaks. The mutual positions of the peaks are influenced by the energy shifts in the STS measurement due to the tip-induced band bending and electron-transport problems. We expect pronounced variations in the fine structure of the height difference for measurements where the tip-induced band bending, or electron transport differ from the presented measurement, i.e., for different tips, different Bi-Ge-Si surfaces (mixed vs homogeneous), or different temperatures.

C. Height difference vs local work function

Local changes in the work function as a reason for the height difference in STM have been mentioned in the earliest accounts of the STM technique.[44] More generally, the work function of the sample is one of the several contributions to the local tunneling barrier height (LBH) that determines the magnitude of the tunneling current I_t. The contributions become apparent on the schematic in Fig. 4, where the local tunneling barrier is plotted in a trapezoidal approximation. The LBH is a function of the material parameters of the sample (bulk Fermi level E_F and electron affinity χ) and the tip (work function ϕ_M) and of the parameters of the tunneling contact: sample bias eV_s and tip-induced band bending φ_0. The present work shows that the contribution of φ_0 to the local tunneling barrier height can be significant.[45]

In binary systems, the evidence of the STM contrast based on the local work function of the sample is sporadic.[10] An intriguing STM contrast mechanism related to the local work function has been described in Ref. 12. Rather than on the direct influence of changes in local work function on I_t the study focuses on the localized electron states that form between the STM tip and the investigated surface for higher V_s.[26,27] The energy spectrum of these states is a sensitive

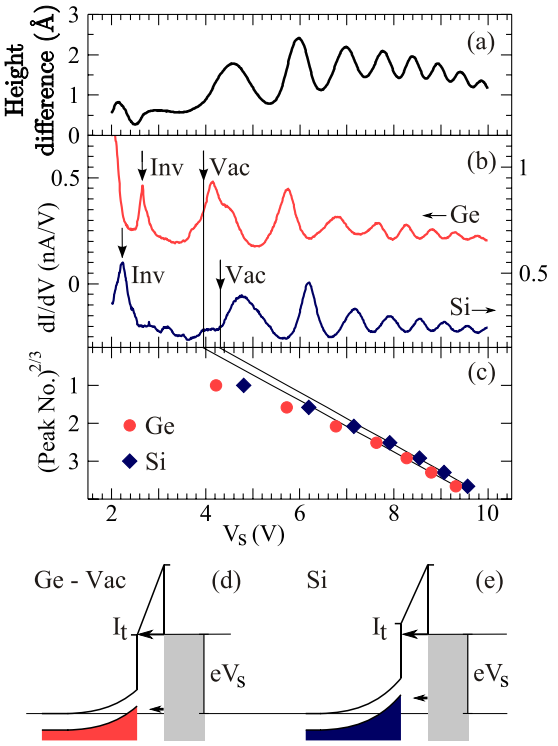

FIG. 5. (Color online) (a) Height difference between clean (Si) and Ge-terminated (Ge) Si(111)-$\sqrt{3}\times\sqrt{3}$-Bi measured in STM at higher sample voltage. Tunneling current 0.1 nA. (b) Corresponding STS signal measured over clean (Si) and Ge-terminated areas. Bulk inversion (Inv) and vacuum oscillations (Vac) thresholds are marked by arrows. (c) Linear fit to the positions of higher-lying vacuum oscillations for determining the position of Vac (cf. Ref. 48). [(d) and (e)] The weaker tip-induced band bending in Ge [cf. Figs. 3(c) and 3(d)] causes that with increasing V_s, the crossing of the vacuum level will be observed first in Ge: compare (d) and (e) for the same V_s in Ge and Si. For the same V_s, the LBH over Ge areas is smaller.

measure of the local tunneling barrier height and STM imaging of these states can yield a very high STM contrast with a characteristic periodic dependence on V_s.[12]

We observe this type of STM contrast between Ge and Si areas at $V_s > 4$ V. The dependence of the STM contrast on V_s is shown in Fig. 5(a). Between $V_s = 2$ V and 4 V the contrast follows the V_s dependence shown in Fig. 2. At $V_s > 4$ V an onset of the contrast is observed with height difference reaching 2 Å at 4.5 V and 2.5 Å at 6 V. The contrast features a modulation in V_s characteristic of the presence of the localized electron states in the tunneling gap. Corresponding STS spectra measured separately on the Ge and the Si areas are shown in Fig. 5(b). The spectra feature the Inv peak belonging to the bulk inversion and identified in Sec. III B and Fig. 3(a) and peaks belonging to the electron resonances between the tip and the sample.[26,27] The resonances on Ge areas are shifted to lower V_s than on Si areas.

The positions of the resonances in Si and Ge STS allow us to make conclusions regarding the profile of the tunneling barrier between the tip and the sample. We assume a trapezoidal tunneling barrier as in Fig. 4. The trapezoidal barrier can be regarded as an envelope of a real barrier. The real barrier is lowered with respect to the trapezoidal barrier in the vicinity of the electrodes, typically due to image forces acting on the tunneling electrons.[46] This lowering does influence the position of the electron resonances between the tip and the sample and must be accounted for in realistic simulations of the resonances in STS spectra.[47] Practically, however, Ref. 48 demonstrated that this lowering affects mostly the first few resonances, and the positions of the higher resonances can be used to reconstruct the profile of the trapezoidal envelope of the tunneling barrier. Positions of the higher lying resonances in STS satisfy for STS acquisition at I_t = const, $E_n = E_{vac} + \beta n^{2/3}$, where n is the number of the resonance peak, E_n is the energy of the peak, β is a measure of the electric field between the tip and the sample, and E_{vac} is the vacuum level on the sample surface (for electrons tunneling into the sample). The vacuum level on the sample surface represents a threshold for the onset of the vacuum oscillations: the oscillations appear for $eV_s > E_{vac}$ (Fig. 4).[26,27]

The vacuum level of the sample can thus be estimated from an intercept of a linear fit of E_n with respect to $n^{3/2}$. We show this fit performed separately for Ge and Si and for $n = 4-7$ in Fig. 5(c). We obtain $E_{vac}^{Ge} = 3.9$ eV for Ge and $E_{vac}^{Si} = 4.3$ eV for Si. We mark the vacuum level as "Vac" in Fig. 5(b). The position of the Vac suggests that, effectively, the local work function on the Ge-terminated areas is smaller than on the Si areas of the Si(111)-$\sqrt{3}\times\sqrt{3}$-Bi surface.

The Inv and the Vac features in the STS spectra of Ge and Si show a very characteristic behavior: when changing from Ge to Si, the Inv peak moves to lower V_s while the Vac peak moves to higher V_s. This can be considered as a fingerprint of a different band bending in Ge and Si areas.[49] As has been discussed in Sec. III B the positions of the Inv peak in Ge and Si tunneling spectra indicate a lower band bending in Ge [cf. Figs. 3(c) and 3(d)]. When increasing V_s further, the lower band bending in Ge causes the effect that the crossing of the sample vacuum level by tip Fermi level appears first in Ge and only later in Si. We show the corresponding schematic in Figs. 5(d) and 5(e). From the schematic it also becomes clear that electrons tunneling on Ge areas are passing a lower tunneling barrier than those tunneling on Si areas.

In the discussion above, we assume that the electron affinity χ is the same for Ge and Si areas, and the positions of the Vac are determined by a lower band bending in Ge areas. In such a model, the band bending is independent of χ. Alternatively, a model can be considered where the electron affinity of Ge differs from that of Si, $\chi_{Ge} \neq \chi_{Si}$, and the band bending is determined by χ. Within the alternative model, the appearance of the Vac at lower V_s in Ge than in Si can be expected in case that $\chi_{Ge} < \chi_{Si}$. However, this implies increasing the φ_0^{Ge} with respect to φ_0^{Si} for the same V_s, and an appearance of the Inv peak at lower V_s in Ge than in Si in contradiction with our experimental observations. The lower tunneling barrier height observed in Ge than in Si areas is thus predominantly determined by the lower band bending in Ge areas.

The local tunneling barrier height is related to the decay length κ of the tunneling current I_t, $\kappa \propto \sqrt{\text{LBH}}$. κ is easily measured as a function of V_s that allows us to obtain conclusions on the V_s dependence of the LBH. We show the V_s

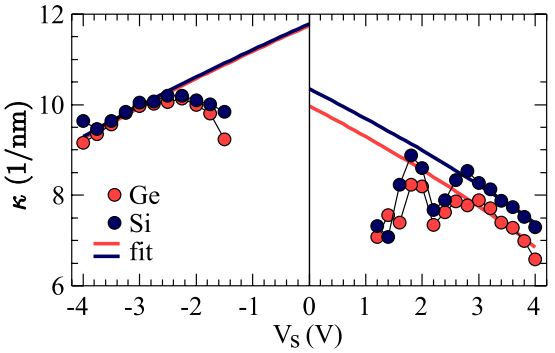

FIG. 6. (Color online) Apparent barrier height expressed as inverse decay length κ of the tunneling current measured over clean (Si) and Ge-terminated (Ge) Si(111)-$\sqrt{3}\times\sqrt{3}$-Bi as a function of V_s (points). For higher absolute voltages $|V_s|\geq 3$ V measured dependence can be fitted by a dependence expected for ideal trapezoidal barrier (thick lines). A difference between Si and Ge is apparent in unoccupied states ($V_s>0$ V), in occupied states it vanishes.

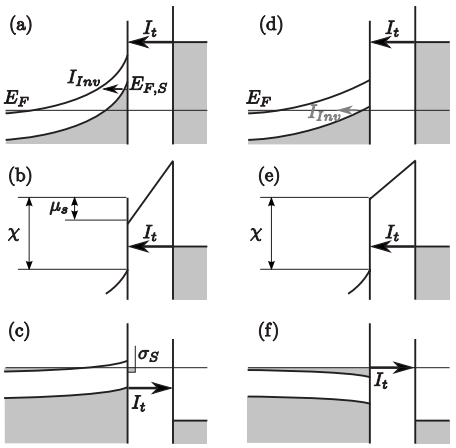

FIG. 7. [(a)–(c)] Mechanisms included in the model of tunneling on Si(111)-$\sqrt{3}\times\sqrt{3}$-Bi. (a) Nonequilibrium tunneling and strong inversion current I_{Inv}, (b) surface dipole μ_s, (c) surface state σ_s and tunneling from the valence band. [(d)–(f)] Counterexamples of (a)–(c): (d) equilibrium tunneling and vanishing I_{Inv}, (e) absence of surface dipole, (f) accumulation layer and tunneling from the conduction band.

dependence of κ in Fig. 6. We can see that a lower κ/lower tunneling barrier height is observed on the Ge areas compared to Si areas for most $V_s>0$ V. The difference between κ/tunneling barrier height on Ge and Si areas decreases or vanishes for most $V_s<0$ V. This asymmetry of Ge-Si κ difference with respect to tunneling in the unoccupied and the occupied states indicates a close relation of the observed difference of the local tunneling barrier height between Ge and Si areas to the tip-induced band bending as well. The Ge-Si κ difference is pronounced in unoccupied states where the band bending in n-doped substrate is large, and it vanishes in occupied states where the band banding is small.[31]

The asymmetry of the Ge-Si κ difference corresponds well with the overall shape of the V_s dependence of the STM contrast between Ge and Si for $|V_s|<4$ V (Fig. 2). A larger contrast is observed for unoccupied states where the tunneling over Ge is facilitated by the observed lowering of κ/local tunneling barrier height, and smaller contrast for occupied states where the κ for Ge and Si areas is the same. However, there is virtually no correlation of the fine structure of the V_s dependence of the STM contrast (kinks in Fig. 2) and the Ge-Si κ difference. Thus, the contribution of the barrier height difference to the STM contrast for $|V_s|<4$ V seems to be rather weak. The barrier height difference becomes significant to the STM contrast for $V_s>4$ V where it induces an energy shift of the electron resonances in the tunneling gap on Ge and Si, and, consequently, a very high STM contrast of up to 2.5 Å at $V_s=6$ V.

D. Tunneling on Si(111)-$\sqrt{3}\times\sqrt{3}$-Bi

In this section we propose a model of tunneling on Si(111)-$\sqrt{3}\times\sqrt{3}$-Bi and discuss mechanisms behind the differences in band bending on the Ge and the Si areas. The starting point for the discussion will be the V_s dependence of κ (Fig. 6). In many published experiments, the measurements of κ have been obscured by electron-transport limitations of various origin that tend to reduce the κ (Refs. 50–53). This seems to be a case in our measurements as well for $|V_s|<3$ V. However, for higher $|V_s|>3$ V where the transport limitations are becoming less relevant the κ fits reasonably well to the expression for tunneling through a trapezoidal barrier,[35] $\kappa=[\frac{2m_e}{\hbar^2}(\phi_{av}-\frac{|eV_s|}{2})]^{1/2}$ with ϕ_{av} an average of the work function of the sample and the tip.

We plot the fit in Fig. 6 separately for Ge and Si and for occupied and unoccupied states. In occupied states, the fits for Ge and Si are equal with $\phi_{av}^{\mathrm{Ge}^-}=\phi_{av}^{\mathrm{Si}^-}=5.3$ eV. In unoccupied states, the corresponding values of $\phi_{av}^{\mathrm{Ge}^+}$ and $\phi_{av}^{\mathrm{Si}^+}$ are more than 1 eV lower, and the difference between Ge and Si is becoming apparent with $\phi_{av}^{\mathrm{Ge}^+}=3.8$ eV smaller than $\phi_{av}^{\mathrm{Si}^+}=4.1$ eV. The discontinuity of the ϕ_{av} at $V_s=0$ V is an artifact of the selected approximation for κ, however, we are referring to it in the present discussion since it conveniently describes the asymmetry of κ with respect to V_s, and at $|V_s|>3$ V.

In the consideration above, the tip-induced band bending present in tunneling on Si(111)-$\sqrt{3}\times\sqrt{3}$-Bi was not included. In the approximation of the trapezoidal tunneling barrier, the tip-induced band bending φ_0 adds to the local barrier height and the evaluation of κ becomes $\kappa=[\frac{2m_e}{\hbar^2}(\phi_{av}+\frac{\varphi_0}{2}-\frac{|eV_s|}{2})]^{1/2}$ (cf. Fig. 4). We recalculate the κ using evaluations of φ_0 obtained from a suitable model of tip-induced band bending [software SEMITIP,[29,54] Version 3]. To mimic the tunneling behavior of the system properly, several assumptions about specific processes present in tunneling on Si(111)-$\sqrt{3}\times\sqrt{3}$-Bi are made. These assumptions are included in the model of tunneling on Si(111)-$\sqrt{3}\times\sqrt{3}$-Bi and are shown schematically in Figs. 7(a)–7(c). Particularly, the nonequilibrium tunneling [Fig. 7(a)], the presence of a surface dipole [Fig. 7(b)], and the pinning of the tip-induced band bending by a CB surface state [Fig. 7(c)] are considered. The recalculated values of κ are shown in Fig. 8.

The assumption of the nonequilibrium tunneling with surface Fermi level $E_{F,S}$ above the bulk Fermi level E_F

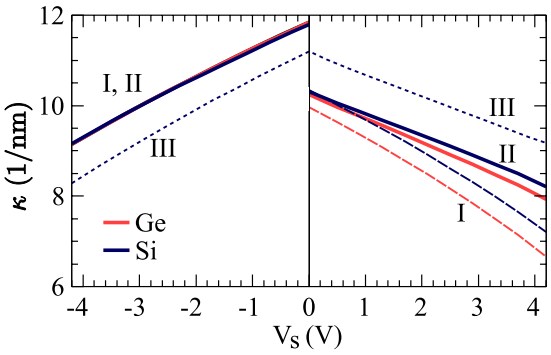

FIG. 8. (Color online) Models of κ based on the evaluation of a trapezoidal barrier. (I) fit to experimental data from Fig. 6. (II) Calculation including tip-induced band bending, the presence of a surface dipole [Fig. 7(b)], and the pinning of the tip-induced band bending by a CB surface state [Fig. 7(c)]. The difference between Ge and Si is modeled using a different dielectric constant of the bulk. (III) Calculation without surface dipole and without pinning [Figs. 7(e) and 7(f)].

[Fig. 7(a)] (Refs. 29 and 31) allows us to properly describe the behavior of the Inv and the Vac peaks in Ge and Si STS (Sec. III C). The difference in the position of the Vac peaks in Si and Ge requires a significant difference in the tip-induced band bending φ_0 in Si and Ge at sample voltages V_s far above the observed inversion threshold Inv. Such difference in φ_0 is difficult to achieve in the case of the equilibrium tunneling [Fig. 7(d)] where $E_{F,S}=E_F$. In such case, after V_s reaching the inversion threshold Inv, the valence-band states are becoming depopulated and the charge associated with the emerging hole gas pins the φ_0 to a value slightly larger than the bulk band gap E_G, $\varphi_0 \approx E_G$,[28] on both Si and Ge areas. In the nonequilibrium tunneling, the depopulation of the valence-band states due to tip-induced band bending is suppressed and φ_0 can grow beyond E_G [Fig. 7(a)]. Nonequilibrium tunneling is typically a result of a limited electron transport between VB and CB. In extreme cases of large bulk band gap and low dopant concentrations (Ref. 28 for GaAs), no inversion current is flowing, however, for smaller band gaps and higher dopant concentrations (Ref. 29 for Ge) the inversion current is becoming measurable as in our experiment. Actually, the nonequilibrium tends to enhance the inversion current because for the electrons at surface Fermi level above bulk Fermi level the tunneling barrier in the space-charge region becomes significantly narrower [cf. Figs. 7(a) and 7(b)].[31] In the present calculation of φ_0 and κ we use an assumption of extreme nonequilibrium with surface Fermi level at VBM, however, in reality the positioning of $E_{F,S}$ between E_F and surface VBM can be expected.[29]

The presence of a surface dipole [Fig. 7(b)] and the pinning of the tip-induced band bending by a CB surface state [Fig. 7(c)] allow us to account for the difference in ϕ_{av} observed for tunneling between occupied and unoccupied states (cf. Fig. 6). The pinning of the tip-induced band bending by a CB surface state suppresses the formation of the accumulation space charge that is expected for tunneling in occupied states at $V_s<0$ V [Fig. 7(f), Refs. 55 and 56]. This, in turn, causes the effect that the tunneling current in occupied states comes predominantly from the valence-band states, and the ϕ_{av}^- increases with respect to ϕ_{av}^+ by $\approx \frac{1}{2}E_G$.[57] The Si(111)-$\sqrt{3}\times\sqrt{3}$-Bi surface has a suitable CB surface state, the free-electronlike surface state predicted by the *ab initio* calculations.[24] The surface state has an onset 0.2 eV below CBM, and an estimated surface density of states 1.4×10^{14} cm^{-2} eV^{-1}.[58] Including the parameters of the surface state into the calculation of φ_0 causes pinning of the CBM above E_F for all considered $V_s<0$ V. For $V_s>0$ V, the surface state is unoccupied and does not influence the φ_0.

Increasing the difference between ϕ_{av}^- and ϕ_{av}^+ beyond $\frac{1}{2}E_G$ requires an additional reduction in ϕ_{av}^+. This can be tentatively attributed by including a dipole layer with a potential drop μ_s at the Si(111)-$\sqrt{3}\times\sqrt{3}$-Bi surface [Fig. 7(b)] effectively reducing the ϕ_{av} by $\frac{1}{2}\mu_s$. Surface dipole layers lowering the local work function in the order of 1 eV are commonly observed[47,59] and can be expected also for the Si(111)-$\sqrt{3}\times\sqrt{3}$-Bi surface where a charge transfer from Bi dangling bonds to Si backbonds occurs.[25] Specific about the Si(111)-$\sqrt{3}\times\sqrt{3}$-Bi surface dipole is that it must be vanishing for large negative V_s and thus have a strong electric field induced component.[60] This may point to a strong electric polarizability of the Si(111)-$\sqrt{3}\times\sqrt{3}$-Bi surface but, alternatively, to an intrinsic electron-transport limitation as well.[61] In our calculation, we make the simplest approximation $\mu_s=0$ for $V_s<0$ V and $\mu_s=$const for $V_s>0$ V.

We show the recalculated values of κ including tip-induced band bending as curve II in Fig. 8. For comparison, the fit to the experimental data from Fig. 6 is repeated in Fig. 8 as curve I. Dark curves refer to clean Si(111)-$\sqrt{3}\times\sqrt{3}$-Bi surface. The material parameters of the tunneling contact correspond to the used substrate and tip [degenerate doping with 1.6×10^{19} cm^{-3} As, E_F above CBM by $\Delta E_F=0.05$ eV, Si electron affinity $\chi=4.05$ eV, $E_G=1.15$ eV, tip work function 5.4 eV (platinum)]. The tip-sample distance 1 nm, the tip radius 50 nm, and surface dipole $\mu_s=1.8$ eV were selected to obtain a reasonable agreement of κ with experiment. For $V_s<0$ V the curve II coincides with the experimental κ including the calculated $\phi_{av}^{Si^-}=5.3$ eV. For $V_s>0$ V, the calculated $\phi_{av}^{Si^+}=4.1$ eV corresponds to the experimental one, however, the slope of the calculated V_s dependence of κ differs from the experimental one due to inclusion of φ_0 that increases with increasing V_s. Altering the slope of the calculated κ dependence would require further assumptions about the surface dipole μ_s and/or tip-induced band bending φ_0 beyond present qualitative discussion. For reference, we plot in Fig. 8 a curve III that is a calculation of κ without the surface dipole [Fig. 7(e)] and without the VB current [Fig. 7(f)]. Without these assumptions, the difference between ϕ_{av}^- and ϕ_{av}^+ obtained in fitting the experimental data in Fig. 6 is not reproduced.

So far, processes playing a role in tunneling on clean Si(111)-$\sqrt{3}\times\sqrt{3}$-Bi have been discussed. Obtaining the Ge-Si difference of the calculated κ requires a further modification of the model. Based on the discussion in Sec. III C we are looking for a mechanism accounting for the better screening of the electric field of the tip on the Ge areas. The desired mechanism would induce a lower band bending in Ge than in Si without requiring a difference of the electron affinity or surface dipole between Ge and Si areas.

Most generally, the better screening of the electric field on Ge areas can be modeled considering a different dielectric constant of the bulk for the Ge areas. We evaluate such an effect using the above described calculation and substituting the bulk dielectric constant 11.8 (Si) by 16 (Ge) while keeping the other parameters unchanged. We show the resulting κ for Ge as curve II, red (light) part, in Fig. 8. The difference of the dielectric constant yields a difference of κ in a qualitative agreement with the experiment. κ for Ge is lower than for Si and this lowering is a function of the band bending. In unoccupied states the lowering is significant and in occupied states it vanishes. We can estimate the positions of Inv and Vac peaks from the calculation. Inv occurs at V_s when $\varphi_0 = E_G + \Delta E_F$, Vac occurs when $eV_s = \varphi_0 + \chi - \mu_s - \Delta E_F$. The characteristic behavior of the Inv and the Vac peaks in Ge and Si is reproduced, the calculated V_s of the Inv and the Vac peaks for curve II and Ge (3.0 and 3.6 V) being between the Inv and the Vac peaks for curve II and Si (2.2 and 4.0 V) in agreement with the experiment.

A difference of the dielectric constants of Ge and Si areas was taken as the simplest example of a mechanism that alters the tip-induced band bending without directly influencing the surface dipole. It is a simplification, since an eventual difference in dielectric constants between Ge and Si areas will be effective only in a few subsurface monolayers. Other mechanisms yielding the correct characteristic behavior of the Inv and the Vac peaks may contribute to the lowering of κ for $V_s > 0$ V. An example of such a mechanism would be a depopulation of the v_1 state in Ge in the proximity of the Inv transition. This would induce a positive surface charge and contribute to a better screening of the electric field of the tip for unoccupied states in Ge areas. Distinguishing the effective mechanisms behind the observed differences in the tip-induced band bending would, however, require a study based on a broader set of experimental data than presented in this work.

IV. CONCLUSIONS

We studied the voltage (V_s) dependence of the STM contrast between Ge- and Si-terminated areas on the Si(111)-$\sqrt{3}\times\sqrt{3}$-Bi surface using low-temperature STM and STS techniques. Ge-terminated areas appear higher than Si-terminated areas for most V_s and the height difference becomes much more pronounced for tunneling into the unoccupied states. We find that for lower sample bias $|V_s| < 3$ V the voltage-dependent STM contrast correlates exceptionally well with the difference between voltage-integrated STS curves measured on Ge- and Si-terminated areas. The STM contrast is influenced both by density-of-state features, and other effects, especially the electron-transport limitations and tip-induced band bending. We propose that true density-of-states contributions influence the overall shape of the V_s dependence of the STM contrast, especially a strong onset at $V_s \approx 2$ V that correlates with a pronounced peak in Ge STS.

Our measurements indicate a smaller tip-induced band bending on Ge than on Si areas. The difference in the band bending manifests itself uniquely through specific positions of non-density-of-state features in STS spectra, the Inv peak belonging to the onset of tunneling through the depletion layer in sample bulk (appears at higher V_s on Ge areas compared to Si areas), and the Vac peak belonging to the crossing of the sample vacuum level by the tip Fermi level (appears at lower V_s on Ge areas compared to Si areas).

This difference in the band bending causes an effective difference in the local tunneling barrier height measured by STM that becomes proportional to the band bending, and thus dependent on V_s. For unoccupied states, the local tunneling barrier height becomes smaller on Ge areas than on Si areas. For occupied states, the difference in the local tunneling barrier height vanishes. We construct a simple model of the tip-induced band bending showing that the characteristic difference in the band bending observed in our experiment can be explained by a higher dielectric constant of the Ge areas.

The difference in the local tunneling barrier height measured by STM strongly influences tunneling on Ge and Si areas at $V_s > 3$ V where localized electron states form between the sample and the STM tip. The differences between these states on Ge and Si areas cause a second strong onset of the STM contrast at $V_s \approx 4$ V, and characteristic oscillations of this contrast at $V_s > 4$ V.

ACKNOWLEDGMENTS

We would like to thank Vasily Cherepanov, Neelima Paul, and Kurt Schroeder for many helpful discussions and Helmut Stollwerk and Peter Coenen for the expert technical assistance. J.M. acknowledges the support of the research Program No. MSM 0021620834 of the Ministry of Education of the Czech Republic. F.D. acknowledges the support of the research Program No. GAUK 92209 of the Grant Agency of the Charles University. A.S. acknowledges the support of European Union FP6 project NANOCAGE (Grant No. MEST-CT-2004-50-6854).

*Author to whom correspondence should be addressed; josef.myslivecek@mff.cuni.cz

†Present address: Institut für Experimentalphysik, Freie Universität Berlin, Arnimallee 14, 14195 Berlin, Germany.

[1] J. Tersoff and D. R. Hamann, Phys. Rev. Lett. **50**, 1998 (1983); Phys. Rev. B **31**, 805 (1985).

[2] C. J. Chen, *Introduction to Scanning Tunneling Microscopy* (Oxford University Press, Oxford, 2008).

[3] R. M. Feenstra, J. A. Stroscio, J. Tersoff, and A. P. Fein, Phys. Rev. Lett. **58**, 1192 (1987).

[4] M. Schmid, H. Stadler, and P. Varga, Phys. Rev. Lett. **70**, 1441 (1993).

[5] B. Voigtländer, V. Scheuch, H. P. Bonzel, S. Heinze, and S. Blügel, Phys. Rev. B **55**, R13444 (1997).

[6] A. Davies, J. A. Stroscio, D. T. Pierce, and R. J. Celotta, Phys. Rev. Lett. **76**, 4175 (1996).

[7] M. M. J. Bischoff, T. K. Yamada, and H. van Kempen, Phys. Rev. B **67**, 165403 (2003).

[8] M. Švec, P. Jelínek, P. Shukrynau, C. González, V. Cháb, and V. Drchal, Phys. Rev. B **77**, 125104 (2008).

[9] T. Trappmann, M. Gajdzik, C. Sürgers, and H. v. Löhneysen, Europhys. Lett. **39**, 159 (1997).
[10] G. Gilarowski, J. Méndez, and H. Niehus, Surf. Sci. **448**, 290 (2000).
[11] Y. W. Mo and F. J. Himpsel, Phys. Rev. B **50**, 7868 (1994).
[12] T. Jung, Y. W. Mo, and F. J. Himpsel, Phys. Rev. Lett. **74**, 1641 (1995).
[13] F. Schäffler, Semicond. Sci. Technol. **12**, 1515 (1997); A. D. Yoffe, Adv. Phys. **50**, 1 (2001); B. Voigtländer, Surf. Sci. Rep. **43**, 127 (2001).
[14] X. R. Qin, B. S. Swartzentruber, and M. G. Lagally, Phys. Rev. Lett. **84**, 4645 (2000).
[15] D.-S. Lin, J.-L. Wu, S.-Y. Pan, and T.-C. Chiang, Phys. Rev. Lett. **90**, 046102 (2003).
[16] M. Kawamura, N. Paul, V. Cherepanov, and B. Voigtländer, Phys. Rev. Lett. **91**, 096102 (2003).
[17] M. Horn-von Hoegen, F. J. Meyer zu Heringdorf, M. Kammler, C. Schaeffer, D. Reinking, and K. R. Hofmann, Thin Solid Films **343-344**, 579 (1999).
[18] N. Paul, H. Asaoka, J. Mysliveček, and B. Voigtländer, Phys. Rev. B **69**, 193402 (2004).
[19] V. Cherepanov, S. Filimonov, J. Mysliveček, and B. Voigtländer, Phys. Rev. B **70**, 085401 (2004).
[20] N. Paul, S. Filimonov, V. Cherepanov, M. Cakmak, and B. Voigtländer, Phys. Rev. Lett. **98**, 166104 (2007).
[21] K. Romanyuk, J. Mysliveček, V. Cherepanov, T. Sekiguchi, S. Yoshida, K. M. Itoh, and B. Voigtländer, Phys. Rev. B **75**, 241309 (2007).
[22] K. Romanyuk, J. Brona, and B. Voigtländer, Phys. Rev. Lett. **103**, 096101 (2009).
[23] K. Romanyuk, V. Cherepanov, and B. Voigtländer, Phys. Rev. Lett. **99**, 126103 (2007).
[24] R. H. Miwa, T. M. Schmidt, and G. P. Srivastava, J. Phys.: Condens. Matter **15**, 2441 (2003).
[25] R. H. Miwa, T. M. Schmidt, and P. Venezuela, Phys. Rev. B **72**, 125403 (2005).
[26] R. S. Becker, J. A. Golovchenko, and B. S. Swartzentruber, Phys. Rev. Lett. **55**, 987 (1985).
[27] R. S. Becker, J. A. Golovchenko, D. R. Hamann, and B. S. Swartzentruber, Phys. Rev. Lett. **55**, 2032 (1985).
[28] N. D. Jäger, E. R. Weber, K. Urban, and Ph. Ebert, Phys. Rev. B **67**, 165327 (2003).
[29] R. M. Feenstra, S. Gaan, G. Meyer, and K. H. Rieder, Phys. Rev. B **71**, 125316 (2005).
[30] B. Voigtländer, V. Cherepanov, C. Elsaesser, and U. Linke, Rev. Sci. Instrum. **79**, 033911 (2008).
[31] J. Mysliveček, A. Stróżecka, J. Steffl, P. Sobotík, I. Ošt'ádal, and B. Voigtländer, Phys. Rev. B **73**, 161302 (2006).
[32] P. Mårtensson and R. M. Feenstra, Phys. Rev. B **39**, 7744 (1989).
[33] J. A. Stroscio, R. M. Feenstra, and A. P. Fein, Phys. Rev. Lett. **57**, 2579 (1986).
[34] R. M. Feenstra, J. A. Stroscio, and A. P. Fein, Surf. Sci. **181**, 295 (1987).
[35] J. A. Stroscio, R. M. Feenstra, D. M. Newns, and A. P. Fein, J. Vac. Sci. Technol. A **6**, 499 (1988).
[36] R. Shioda, A. Kawazu, A. A. Baski, C. F. Quate, and J. Nogami, Phys. Rev. B **48**, 4895 (1993).
[37] J. C. Woicik, G. E. Franklin, C. Liu, R. E. Martinez, I.-S. Hwong, M. J. Bedzyk, J. R. Patel, and J. A. Golovchenko, Phys. Rev. B **50**, 12246 (1994).
[38] R. Z. Bakhtizin, Ch. Park, T. Hashizume, and T. Sakurai, J. Vac. Sci. Technol. B **12**, 2052 (1994).
[39] A. Antons, R. Berger, K. Schroeder, and B. Voigtländer, Phys. Rev. B **73**, 125327 (2006).
[40] T. Hirahara, I. Matsuda, M. Ueno, and S. Hasegawa, Surf. Sci. **563**, 191 (2004).
[41] J. Mysliveček (unpublished).
[42] R. M. Feenstra, Surf. Sci. **603**, 2841 (2009).
[43] Given the influence of the tip in STS measurements, however, our proposal is subject to reconfirmation by tip-independent methods for determining LDOS, e.g., photoelectron and inverse photoelectron spectroscopy (Ref. 11), or *ab initio* calculations (Refs. 24 and 25).
[44] G. Binnig and H. Rohrer, Surf. Sci. **126**, 236 (1983).
[45] In Sec. III C, we introduce the relation of φ_0 to the different LBH on Ge and Si areas. In Sec. III D, we discuss the V_s dependence of φ_0 and LBH.
[46] Y. Suganuma and M. Tomitori, J. Vac. Sci. Technol. B **18**, 48 (2000).
[47] H.-C. Ploigt, C. Brun, M. Pivetta, F. Patthey, and W.-D. Schneider, Phys. Rev. B **76**, 195404 (2007).
[48] O. Yu. Kolesnychenko, O. I. Shklyarevskii, and H. van Kempen, Phys. Rev. Lett. **83**, 2242 (1999).
[49] The relation of Inv and Vac to the tip-induced band banding can be seen also from the shifts of Inv and Vac observed without changing the tip position, but after a spontaneous change in the tip geometry. After the tip change, Inv and Vac keep moving in opposite directions. They are approaching each other upon lowering of the tip work function and vice versa.
[50] M. Weimer, J. Kramar, and J. D. Baldeschwieler, Phys. Rev. B **39**, 5572 (1989).
[51] L. Olesen, M. Brandbyge, M. R. Sørensen, K. W. Jacobsen, E. Lægsgaard, I. Stensgaard, and F. Besenbacher, Phys. Rev. Lett. **76**, 1485 (1996).
[52] V. Ramachandran and R. M. Feenstra, Phys. Rev. Lett. **82**, 1000 (1999).
[53] S. Nie, R. M. Feenstra, Y. Ke, R. P. Devaty, and W. J. Choyke, J. Appl. Phys. **103**, 013709 (2008).
[54] http://www.andrew.cmu.edu/user/feenstra/semitip_v3
[55] R. Dombrowski, C. Steinebach, C. Wittneven, M. Morgenstern, and R. Wiesendanger, Phys. Rev. B **59**, 8043 (1999).
[56] R. M. Feenstra, G. Meyer, F. Moresco, and K. H. Rieder, Phys. Rev. B **66**, 165204 (2002).
[57] N. Ishida, K. Sueoka, and R. M. Feenstra, Phys. Rev. B **80**, 075320 (2009).
[58] The density of states is a step function that is zero below the onset energy and constant above the onset energy. The density of states is $m_e/\pi\hbar^2$ with the effective mass m_e of the free surface electron equal to the effective mass of the Si CBM as can be estimated based on the electron structure of the Si(111)-$\sqrt{3}\times\sqrt{3}$-Bi surface shown in Fig. 3(b) of Ref. 24.
[59] F. E. Olsson, M. Persson, J. Repp, and G. Meyer, Phys. Rev. B **71**, 075419 (2005).
[60] R. Akiyama, T. Matsumoto, and T. Kawai, Phys. Rev. B **62**, 2034 (2000).
[61] We observe a difference between ϕ_{av}^{+} and ϕ_{av}^{-} comparable to that on Si(111)-$\sqrt{3}\times\sqrt{3}$-Bi surface also on a Si(111)-7×7 surface before terminating with Bi.